Agitation, Mixing, and Transfers Induced by Bubbles — **Source link** ⬈

Frédéric Risso

Related papers:

- Turbulence in the liquid phase of a uniform bubbly air-water flow

- Experimental characterization of the agitation generated by bubbles rising at high Reynolds number

- Bubbles, Drops, and Particles

- The Motion of High-Reynolds-Number Bubbles in Inhomogeneous Flows

- Gravity-driven bubbly flows

Agitation, Mixing, and Transfers Induced by Bubbles

Frédéric Risso

Institut de Mécanique des Fluides de Toulouse (IMFT), Université de Toulouse, CNRS, INPT, UPS, 31400 Toulouse, France; email: Frederic.Risso@imft.fr

Abstract

Bubbly flows involve bubbles randomly distributed within a liquid. At large Reynolds number, they experience an agitation that can combine shear-induced turbulence (SIT), large-scale buoyancy-driven flows, and bubble-induced agitation (BIA). The properties of BIA strongly differ from those of SIT. They have been determined from studies of homogeneous swarms of rising bubbles. Regarding the bubbles, agitation is mainly caused by the wake-induced path instability. Regarding the liquid, two contributions must be distinguished. The first one corresponds to the anisotropic flow disturbances generated near the bubbles, principally in the vertical direction. The second one is the almost isotropic turbulence induced by the flow instability through a population of bubbles, which turns out to be the main cause of horizontal fluctuations. Both contributions generate a k^{-3} spectral subrange and exponential probability density functions. The subsequent issue will be to understand how BIA interacts with SIT.

1. INTRODUCTION

Bubbly flows belong to the more general family of dispersed two-phase flows, in which a population of particles (either solid, liquid, or gaseous) is dispersed into a fluid, termed the continuous phase. Such flows are complex because the two phases undergo two different, but closely coupled, dynamics.

Two mechanisms can force the motion of the particles to be different from that of the surrounding fluid. First, the fact that the dispersed particles cannot deform as much as the continuous phase produces hydrodynamic forces, so-called Faxén forces (Gatignol 1983). Second, the inertia and gravity forces acting on the particles are different from those acting on the surrounding fluid as soon as the densities of the two phases differ. This latter mechanism is more often dominant, and we focus here on situations where it can be considered as the only cause of velocity differences between particles and the fluid. Furthermore, the existence of a density difference can lead to another major consequence. A single phase is usually set in motion by an imposed external pressure gradient, caused either by a pump or by gravity. A dispersed two-phase flow can also be generated by the sole action of buoyancy, for instance, by pouring heavy particles in a lighter fluid or injecting gas bubbles in a liquid. The existence of two causes of motions leads to a wide range of flow regimes, involving various physical mechanisms (**Figure 1a**). The external pressure gradient and the buoyancy generate mean and fluctuating motions in the liquid and in the dispersed phase.

We first consider the case where buoyancy is negligible compared to the imposed pressure gradient, as is usually the case when small bubbles are dispersed in a liquid pipe flow. The pressure gradient causes a liquid flow, which becomes unstable if the Reynolds number is large enough and generates turbulence, mainly close to the wall. Concurrently, the pressure gradient induces a mean bubble motion, characterized by a velocity that differs from that of the fluid. The shear-induced turbulence (SIT) then causes random motions of the bubbles, and in return, the presence of the bubbles alters the liquid turbulence. These two latter mechanisms are predominant when the SIT is the main source of fluctuations. Their investigation has given rise to a large number of contributions (Balachandar & Eaton 2010) and still remains an issue of major interest for the scientific community. The effect of turbulence on the motion of the bubbles is often called particle dispersion and is referred to as one-way coupling in numerical simulations. It is, in particular, responsible for the preferential concentration of particles in certain regions of the flow. The effect of bubbles on turbulence is often called the turbulence modulation and is referred as two-way coupling in such simulations.

We now consider the opposite situation, in which buoyancy is the only cause of motion, as is the case in bubble columns where gas bubbles are injected at the bottom of a tank filled with a liquid otherwise at rest (**Figure 1b,c**). Buoyancy causes the rising motion of the bubbles, but it induces no mean motion of the liquid phase, provided that the random spatial distribution of the bubbles is uniform. The flow disturbances generated by bubble-rising motions induce velocity fluctuations in the surrounding liquid. This agitation of the liquid is often called bubble-induced turbulence or pseudo-turbulence (Lance & Bataille 1991), but we prefer to call it bubble-induced agitation (BIA), which does not suggest any physical interpretation. Of course, BIA acts in return on the dispersed phase, but it is not the only cause of bubble agitation. Freely rising or falling bodies are observed to follow oscillatory paths when their wake becomes unsteady (Ern et al. 2012). These wake-induced fluctuations represent the major part of bubble agitation for millimeter-sized bubbles in water.

A homogeneous spatial distribution of bubbles represents a very peculiar flow regime, which is hard to observe in industrial bubble columns where large-scale liquid flows develop (Mudde 2005). In spite of these considerations, a homogeneous bubble column can be more easily obtained in laboratory experiments under the condition that bubbles are injected rigorously uniformly
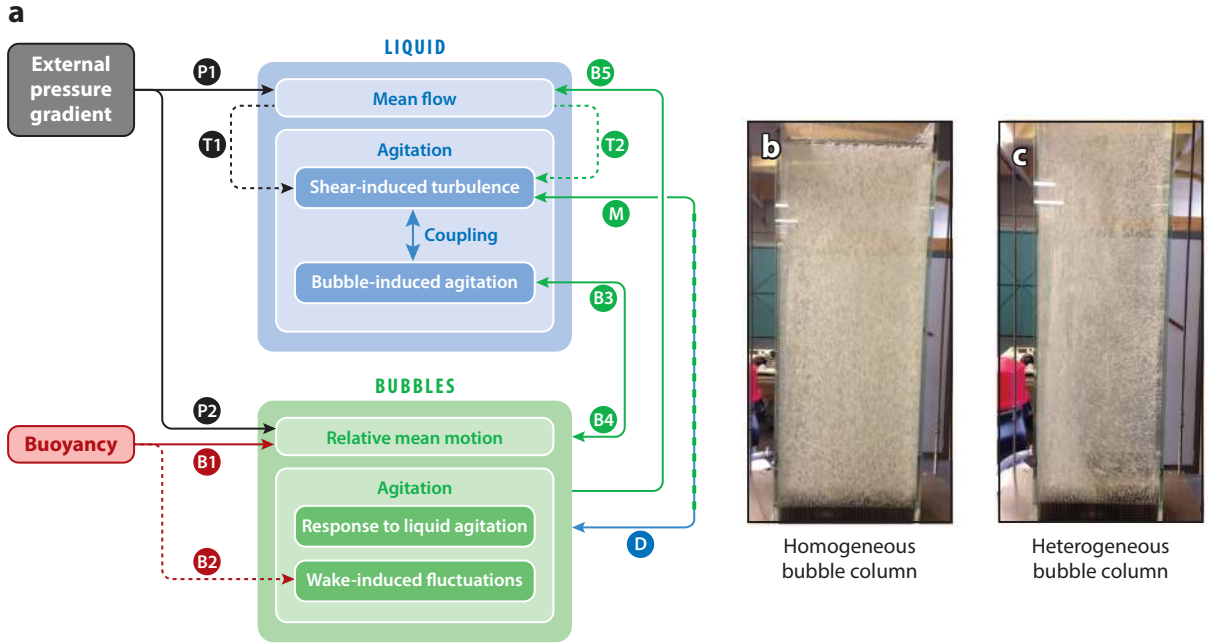
a

LIQUID

External pressure gradient (P1)

Mean flow (B5)

(T1)

Agitation (T2)

Shear-induced turbulence (M)

Coupling

Bubble-induced agitation (B3)

BUBBLES

(P2)

Relative mean motion (B4)

Buoyancy (B1)

Agitation

Response to liquid agitation

(B2)

Wake-induced fluctuations (D)

b

c

Homogeneous bubble column

Heterogeneous bubble column

Figure 1

(*a*) Physical mechanisms involved in a turbulent bubbly flow. There are two possible causes of motions: an imposed external pressure gradient (*black*) and buoyancy (*red*). The pressure gradient causes a mean flow (P1) in the liquid (*blue*), generating near-wall turbulence (T1) if the Reynolds number is large enough. Concurrently, the pressure gradient induces a mean motion (P2) in the dispersed phase (*green*). The shear-induced turbulence causes random motions of the bubbles (D), which in turn alters the liquid turbulence (M). Buoyancy causes the bubbles to rise (B1). The flow disturbances generated by bubble-rising motions induce velocity fluctuations in the surrounding liquid (B3), which acts in return on the dispersed phase (B4). Freely rising or falling bodies follow oscillatory paths when their wakes become unsteady, inducing the major part of agitation for millimeter-sized bubbles in water (B2). Buoyancy may also generate mean liquid flows (B5) through an inhomogeneity of the bubble concentration. As the concentration increases, these motions generate strong liquid velocity gradients that eventually produce turbulence (T2). (*b*) Laboratory-created homogeneous and (*c*) heterogeneous bubble columns.

(Harteveld 2005). For a given column geometry, a homogeneous bubble distribution, which remains stable under moderate spatial perturbations of the bubble injection, can be obtained up to a critical value of the gas volume fraction α (Harteveld & Mudde 2003). This critical value depends on the aspect ratio of the column, and it is possible to recover a stable homogeneous flow from an unstable configuration by decreasing the liquid height in the column (Colombet et al. 2015). Above this threshold, rising motions of the bubbly mixture are observed in regions where the bubble concentration is higher, while downward flows are observed where it is lower. Through an inhomogeneity of the bubble concentration, buoyancy may thus generate mean liquid flows as natural convection does (Climent & Magnaudet 1999). With an increase in the average gas volume fraction, these buoyancy-driven motions become stronger and generate strong liquid velocity gradients that eventually produce turbulent fluctuations. Even if they both originate from the bubbles and exist in the absence of an external pressure gradient, the turbulence induced by the inhomogeneity of bubbles' spatial distribution and the agitation that develops in homogeneous situations require two separate descriptions, each involving different mechanisms. On the one hand, the first mechanism (part T2 of **Figure 1**) involves large-scale motions that give rise to a cascade

of increasingly smaller scales as the buoyancy gradients become larger. It is therefore the same mechanism of turbulence production as single-phase flow (part T1 of **Figure 1**) and generates a turbulence with similar properties. Therefore, it is not distinguished in this review from the SIT that develops in the absence of bubbles. On the other hand, the second mechanism (part B3 of **Figure 1**) injects energy in a narrow range of scales of the order of the bubble size and produces an agitation with statistical properties that are very different from that of classic SIT (Riboux et al. 2010). In the following review, the term BIA refers exclusively to this latter mechanism.

In a pioneering work, Lance & Bataille (1991) injected a homogeneous swarm of bubbles in an upward water flow where SIT was also generated by means of a grid. They clearly showed that the bubbles increased the intensity of the liquid fluctuations and generated an original spectral subrange, where the power spectral density decreased approximately as the −3 power of the wave number. Later, several investigations (reviewed in Rensen et al. 2005) attempted to determine the statistical properties of BIA but found different results, especially regarding the spectrum of the fluctuations. These discrepancies arose from the fact that SIT and BIA were simultaneously present with various relative intensities. To allow relevant comparisons between the various situations, Rensen et al. (2005) introduced the bubblance parameter, which compares the intensity of BIA to that of SIT. Although it is difficult to estimate this parameter in the general case, it can be easily determined in a homogeneous bubbly flow where the intensity of SIT is similar to that measured in the absence of bubbles. In a modern version of the Lance & Bataille (1991) configuration, Prakash et al. (2016) experimentally showed how the specific properties of BIA emerged as the bubblance parameter was increased.

In most practical situations, all mechanisms illustrated in **Figure 1** are present. This is the case for an upward turbulent pipe flow with bubbles large enough to have a significant drift velocity relative to the liquid, a configuration that motivated many experimental investigations (reviewed in Rzehak & Krepper 2013). The dynamics of a heterogeneous bubble column without average vertical liquid flow, even if it might appear simpler, was shown to be quite similar to that of a vertical pipe flow (Mudde & Saito 2001). The origins of the large-scale motions responsible for the generation of SIT, which are either an external pressure gradient (part T1 of **Figure 1**) or a nonuniform distribution of the bubbles (part T2 of **Figure 1**), are of secondary importance. The main point is to distinguish SIT from BIA. The modeling of complex turbulent bubbly flows where these two sources of agitations are present has been essentially developed in the framework of the two-fluid formulation of the Reynolds-averaged Navier–Stokes equations (RANS), where the mean velocity and kinetic energy of both phases are considered continuous. In the simplest class of models, introduced by Sato et al. (1981), the effect of the bubbles on the liquid agitation is accounted for by an additional contribution to the effective turbulent viscosity, while the equations for the kinetic energy k_e and the dissipation rate of the liquid fluctuations ϵ are identical to those taken in a single-phase case. The second class of models, reviewed in Ziegenhein et al. (2017), accounts for BIA by the addition of new terms in the equations for k_e and ϵ. The third class of models introduces a separate equation for the kinetic energy of BIA (Chahed et al. 2003). Even if the third class is more realistic, the second one is nowadays the most commonly used, probably due to the lack of reliable closure laws for BIA and its coupling with SIT.

Understanding turbulent bubbly flows therefore requires a deep knowledge of the agitation generated by a population of bubbles freely moving in a fluid. In the last 15 years, several experimental investigations and numerical simulations of a homogeneous swarm of rising bubbles of fixed size (i.e., in the absence of bubble breakup or coalescence) have converged towards a rather complete description of the specific statistical properties of BIA. Concurrently, researchers have made significant progress regarding the underlying physical mechanisms. The aim of this article is to review these advances by addressing, in particular, the following questions: To what extent is the

dynamics of a single bubble relevant for describing that of a bubble swarm? How are bubble wakes modified by collective effects? Is BIA a real turbulence? What is the origin of the peculiar spectral and statistical features of BIA? How do bubbles mix a tracer or influence interfacial transfers?

2. MOTIONS GENERATED BY INDIVIDUAL BUBBLES

2.1. Motion of a Single Rising Bubble

We first consider the case of a single gas bubble rising in a liquid at rest under the action of gravity because it corresponds to the reference case in the absence of any interactions between the bubbles. Considering a pure liquid and neglecting the density and viscosity of the gas, we find that problem involves five physical parameters: the density ρ and viscosity μ of the liquid, the surface tension σ, the bubble-equivalent diameter $d = (6\vartheta/\pi)^{1/3}$ based on the bubble volume ϑ, and gravity g. Among the dimensionless parameters that can be defined, only two are independent, namely the Eötvos ($\rho d^2 g/\sigma$) and the Morton ($g\mu^4/\rho\sigma^3$) numbers. This elementary situation is already very complex and leads to a wide range of flow regimes (Maxworthy et al. 1996). In practice, the physical analysis of the bubble dynamics is often carried out by considering nondimensional numbers that involve the average bubble rise velocity $\langle V \rangle$: the Reynolds number $Re = \rho\langle V\rangle d/\mu$, the Weber number $We = \rho\langle V\rangle^2 d/\sigma$, and the drag coefficient $C_d = 4gd/3\langle V\rangle^2$.

Figure 2a shows measurements of the mean rise velocity $\langle V \rangle$ of an air bubble rising in pure water as a function of its diameter from Duineveld (1995). The velocity of small bubbles ($d \leq 1$ mm), which are almost spherical and rise on a straight path, increases with d. Larger bubbles take a spheroidal shape (Figure 2b) as the velocity reaches a maximum before decreasing. Concurrently, the bubble wake becomes unstable and bubbles larger than 2 mm generally follow an oscillatory path (Aybers & Tapucu 1969, Ellingsen & Risso 2001, Shew et al. 2006), as shown in Figure 2c. Finally, very large bubbles ($d \gtrsim 10$ mm) take the shape of a hemispherical cap and rise on an almost straight path.

Magnaudet & Mougin (2007) showed from numerical simulations that bubble path oscillations occur when the production of vorticity at the interface exceeds its advection by the flow going around the bubble. They proposed a criterion for the onset of the path instability based on the maximum vorticity magnitude at the interface. This criterion was in agreement with experiments conducted by Zenit & Magnaudet (2008) involving bubbles rising in pure silicone oil and corresponded to a bubble aspect ratio of 2 for $Re > 100$.

In practice, the continuous phase is rarely a totally pure liquid and, especially when it involves water, contains surface-active molecules that adsorb on the bubble surface. Figure 2a also shows two different rise velocities of air bubbles in tap water, as measured in the same experimental setup by Peters & Els (2012). The main discrepancy between the two sets of data lies in the fact that faster bubbles were rapidly released so that surfactant did not have the time to reach the interface, whereas slower bubbles were kept at rest for a few seconds before being released. The velocity decrease of the bubbles can be explained by the presence of a small amount of surfactant, which is a well-known phenomenon largely described in the literature (Takagi & Matsumoto 2011). The adsorbed molecules are advected towards the bubble rear, which generates a gradient of their surface concentration and induces Marangoni stresses that increase the resistance to the bubble motion (Bel Fdhila & Duineveld 1996, Cuenot et al. 1997). Because it increases the vorticity generated at the interface, the presence of surfactant enhances the development of bubble wake and path instabilities, which are consequently often observed even for spherical bubbles.

It is worth noting that wake-induced path oscillations are not marginal phenomena because they cause significant horizontal velocity fluctuations. For example, the standard deviation of the bubble velocity amounts to 30% of the average velocity for an air bubble of 2.5-mm diameter rising
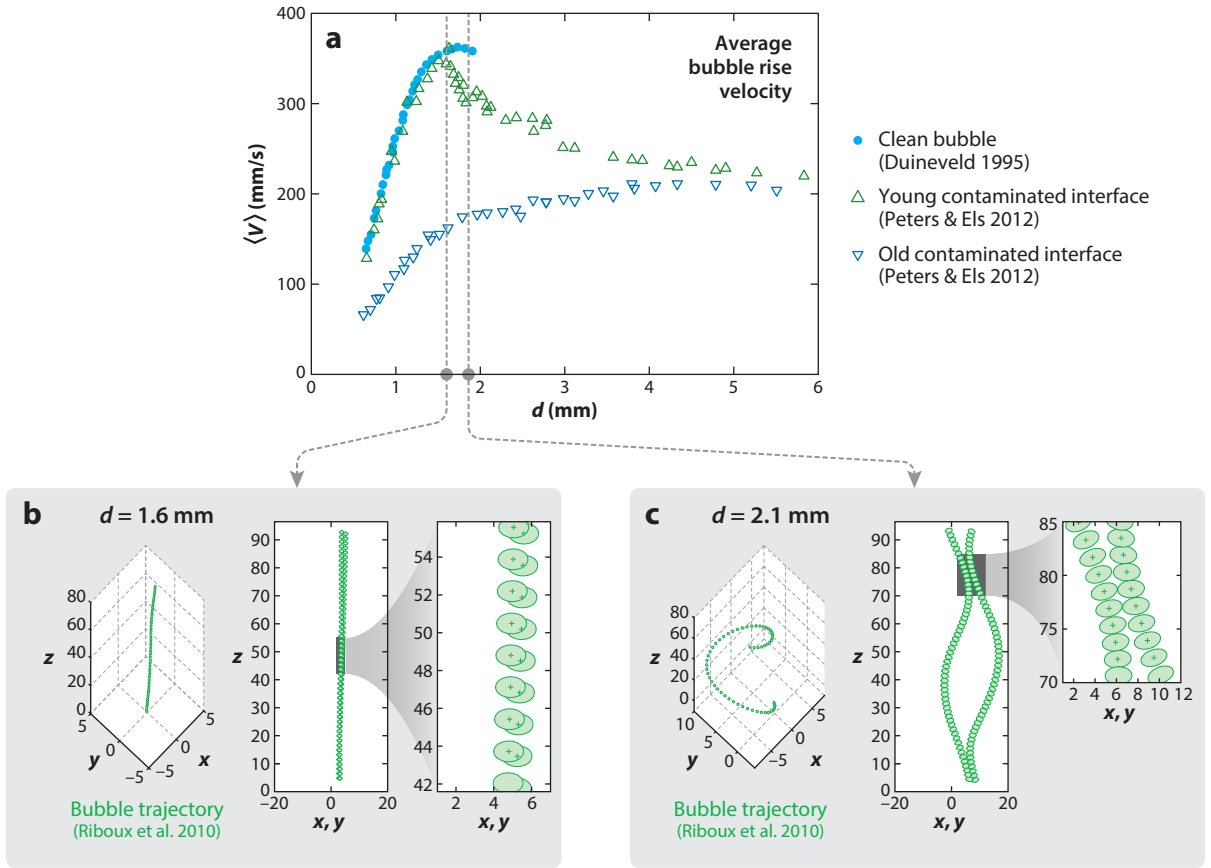
Figure 2

(*a*) Average velocity $\langle V \rangle$ of a single air bubble rising in water as a function of diameter *d*. (*b,c*) Trajectories and shapes of 1.6-mm- and 2.1-mm-diameter single air bubbles rising in water.

in water (Riboux et al. 2010). Moreover, these oscillations are robust, and the velocity fluctuations of a bubble with an unstable wake rising in a turbulent flow are still often dominated by the path instability (Ford & Loth 1998, Mathai et al. 2015).

2.2. Liquid Disturbance Generated by a Bubble

A moving bubble generates a velocity disturbance in the surrounding fluid. At vanishing Reynolds number, the velocity disturbance is a solution of the Stokes equations and decays with the reciprocal of the distance *r* to the bubble (Batchelor 1967, section 4.9). For a clean and spherical bubble at large Reynolds number, the vorticity remains confined in a thin boundary layer and a wake, the thicknesses of which decrease as $Re^{-1/2}$ and $Re^{-1/4}$, respectively (Moore 1963). The potential flow theory therefore gives a good approximation of the flow disturbance, which decays as r^{-3}. However, because large–Reynolds number bubbles are in general not spherical and their interface is often contaminated by surfactant, a significant wake develops behind them (Brücker 1999, Ellingsen & Risso 2001). The mean velocity disturbance in a wake decays with the vertical distance

z to the bubble as z^{-1} in the laminar regime (Batchelor 1967, section 5.12) and as $z^{-2/3}$ in the turbulent one (Tennekes & Lumley 1972, section 4.2).

The flow regime around each bubble thus determines the range of hydrodynamic interactions between bubbles and is of major importance for the dynamics of bubbly flows. A first approximation of the liquid agitation generated in a swarm of bubbles can be sought by neglecting hydrodynamic interactions. Let us consider that the bubble locations are statistically independent from each other and that the liquid velocity in a given location is simply the addition of the flow disturbances induced by each individual bubble. In the Stokes regime, Caflisch & Luke (1985) demonstrated that these assumptions led to an increase without bound of the liquid velocity variance as the size of the swarm increased. Koch & Shaqgeh (1991) showed that a finite variance was obtained if the distribution of the dispersed phase reflected a net deficit in the vicinity of each bubble. Experimental investigations of a homogeneous bubble swarm at low to moderate Reynolds number ($1 \leq Re \leq 50$) conducted by Cartellier & Rivière (2001) and Cartellier et al. (2009) showed the independence of the liquid velocity variance with the size of the bubble swarm and confirmed the existence of a deficit in the bubble distribution near the bubbles. For large–Reynolds number flows, if the flow is assumed to be potential, the addition of independent bubble disturbances allows one to obtain finite values for the variances of the three components of the liquid velocity fluctuations as well as their cross-correlations (Biesheuvel & van Wijngaarden 1984, Lance & Bataille 1991) thanks to the fast decay of the disturbance. However, the addition of individual wakes, decreasing as either z^{-1} or $z^{-2/3}$, leads again to a diverging variance (Parthasarathy & Faeth 1990). Because wakes are the rule rather than the exception, knowledge of the flow disturbances generated by noninteracting bubbles is therefore of little relevance to the description of large–Reynolds number bubbly flows.

Risso & Ellingsen (2002) experimentally investigated the flow disturbance around a bubble immersed in a homogeneous swarm of bubbles for a Reynolds number of 770 and gas volume fractions ranging from 0.5% to 1%. **Figure 3b** shows the evolution of the maximum velocity disturbance with the vertical distance to the bubble for both an isolated bubble ($\alpha = 0$) and a test bubble belonging to a bubble swarm ($\alpha = 0.5\%$). In the close vicinity of the test bubble ($-1 \leq z/d \leq 2.5$), the flow is similar to that of an isolated bubble, potential above it ($z < 0$), and dominated by the wake behind it. For $z/d \geq 2.5$, in contrast with the wake of an isolated bubble that slowly decreases with the distance, the wake of the test bubble is strongly attenuated until almost vanishing at $z/d \approx 5$, where the flow starts to be dominated by homogeneous fluctuations that are independent of the presence of the test bubble. Roig & de Tournemine (2007) measured the average wake behind a bubble within a homogeneous bubble swarm and found that it decreases as $\exp(-z/L_w)$. Risso et al. (2008) showed that the exponential length of decay L_w was almost independent of α and scaled as d/C_d. Moreover, from the investigation of the wake of solid spheres, they found that this exponential decay was not due to an increase of the wake spreading by turbulent diffusion, but rather resulted from interactions between the wakes, as Hunt & Eames (2002) suggested.

Whereas at low to moderate Reynolds numbers ($Re \leq 50$) the intensity of liquid fluctuations is closely related to the microstructure of the bubble spatial distribution, at large Reynolds numbers ($Re \geq 200$) it is governed by wake interactions.

3. STATISTICAL PROPERTIES OF HIGH–REYNOLDS NUMBER HOMOGENEOUS BUBBLE SWARMS

Following Lance & Bataille (1991), several teams designed and built experimental setups able to generate a homogeneous swarm of bubbles having all the same size (Zenit et al. 2001, Garnier
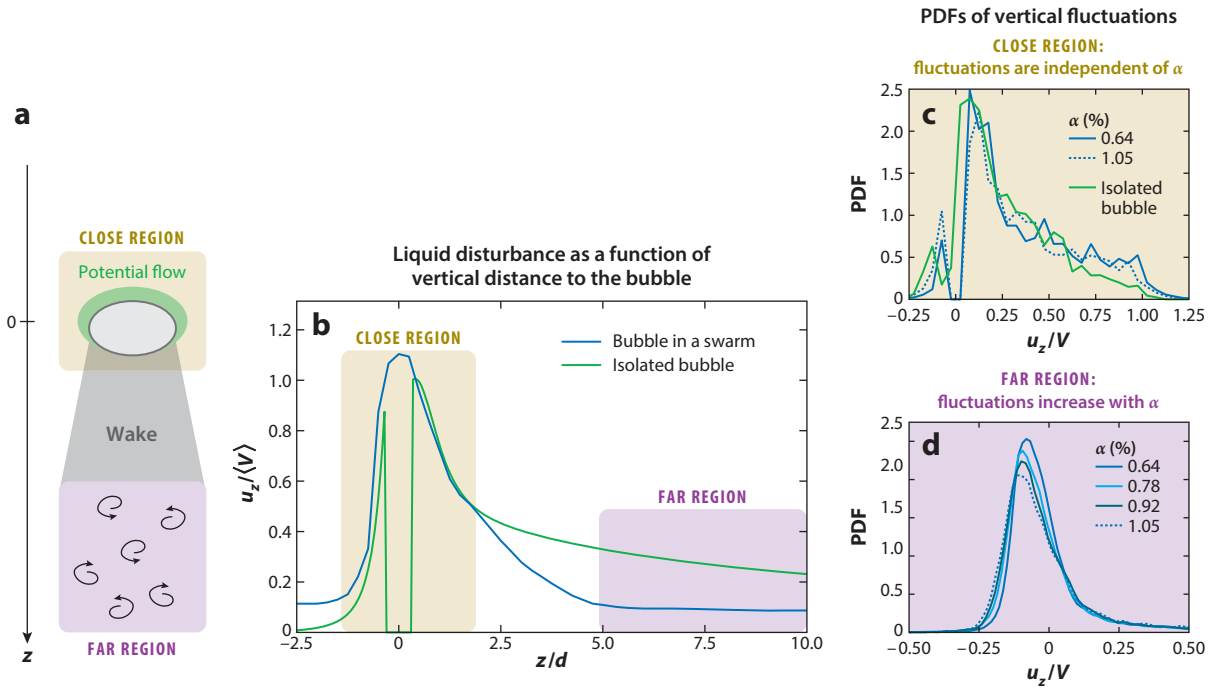
Figure 3

Liquid disturbance generated around a bubble. (*a*) Schematic of the various flow regions. (*b*) Maximum velocity relative to the distance to the bubble. PDFs of the velocity fluctuations close to (*c*) and far from (*d*) a bubble. Abbreviations: α, gas volume fraction; PDF, probability density function.

et al. 2002, Risso & Ellingsen 2002, Rensen et al. 2005), usually by injecting bubbles by means of arrays of calibrated capillary tubes. Various experimental techniques have been used, such as single or multiple optical probes or high-speed imaging for the bubble phase, as well as laser doppler anemometry, hot-film anemometry (HFA) or particle image velocimetry (PIV) for the liquid phase. The presence of interfaces makes measurements much more difficult than in a single-phase flow, disturbing measurements and limiting nonintrusive techniques based on optical imaging to low gas volume fractions. Several solutions were proposed to overcome these limitations, such as adding a small average liquid flow to allow HFA measurements (Garnier et al. 2002, Roig & de Tournemine 2007), using a narrow tank to simplify the use of imaging methods (Zenit et al. 2001), or making measurements below a bubble swarm to facilitate PIV (Riboux et al. 2010). In parallel, swarms of a few tens of bubbles were investigated by means of direct numerical simulations (DNS), first for small or moderate *Re* (Esmaeeli & Tryggvason 1999; Bunner & Tryggvason 2002a,b; Esmaeeli & Tryggvason 2005) and more recently for large *Re* (Roghair et al. 2011b, 2013).

Thanks to continuous efforts and despite the difficulty of comparing results obtained from various methods, the main properties of BIA at large *Re* are now known. They depend on three dimensionless numbers: the Reynolds number that determines the flow regime, the Weber number that governs the bubble shape, and the gas volume fraction that determines the hydrodynamic interactions between bubbles. For a given fluid system, *Re* and *We* are generally varied by changing the bubble diameter, while α is adjusted by varying the inlet gas flow rate.

HFA: hot-film anemometry

PIV: particle image velocimetry

DNS: direct numerical simulation

3.1. Bubble Dynamics

We now describe the dynamics of the dispersed phase by considering the spatial distribution and velocity of the bubbles.

3.1.1. Spatial distribution of the bubbles. In a homogeneous bubble swarm, the average gas volume fraction is spatially uniform. This does not strictly imply that the probability of finding a bubble at a given location is independent of the position of the other bubbles. Due to hydrodynamic interactions, bubbles have a natural tendency to form clusters. DNS of the interaction between two spherical rising bubbles for $50 \leq Re \leq 500$ indicate that the stable position is the side-by-side configuration (Hallez & Legendre 2011). Horizontal bubble clusters were indeed observed in potential flow simulations (Smereka 1993, Yurkovetsky & Brady 1996, Sangani & Didwania 2006) and in DNS considering spherical bubbles at $Re = 91.5$ (Esmaeeli & Tryggvason 2005). However, for deformable bubbles at Re of the order of 100 or higher, such a strong clustering was observed neither in DNS (Esmaeeli & Tryggvason 2005, Roghair et al. 2011b) nor in experiments (Garnier et al. 2002, Roig & de Tournemine 2007, Riboux et al. 2010). Moreover, the statistical distributions of the time intervals between two consecutive bubbles passing at a given point were found to follow a Poisson distribution for homogeneous bubble swarms from $Re = 600$ to 800 and $\alpha = 0.5\%$ to 13% (Risso & Ellingsen 2002, Alméras et al. 2015), indicating that the bubble locations are independent of each other. From accurate measurement of the bubble pair density distribution, Martínez Mercado et al. (2010) nevertheless detected a preferential alignment in the vertical direction at $Re = 1,000$ for small gas volume fractions ($0.28\% \leq \alpha \leq 0.74\%$), which induced long-range correlations ($\geq 20d$) between the bubble locations. This phenomenon is probably related to a mechanism of wake entrainment similar to that revealed by the DNS of Bunner & Tryggvason (2003) for deformable bubbles at moderate Re. The presence of such long-range correlations suggests that the homogeneous swarm was not stable and that a small mean vertical stream was present in the region of measurement. It is also worth mentioning that strong clusters have been observed in more complex situations such as in a confined geometry (Figueroa-Espinoza & Zenit 2005), close to a wall in the presence of surfactant (Takagi et al. 2008), or in non-Newtonian liquids (Vélez-Cordero et al. 2014).

In summary, it can be concluded that no significant clustering is present in homogeneous swarms of nonspherical bubbles rising at large Re. When clusters develop, the homogeneous configuration becomes rapidly unstable and large-scale flows develop. Assuming that the bubble positions are independent of each other is therefore reasonable to derive models of BIA. Because several clustering mechanisms exist, we can wonder why stable bubble columns can be observed at void fractions as large as 30%. In potential flow simulations (Smereka 1993, Yurkovetsky & Brady 1996), it was shown that a significant agitation of the bubbles can prevent the formation of clusters. For large-Re bubbles, the self-induced motions of the bubbles resulting from the wake instability probably constitute the major mechanism that opposes the formation of clusters.

3.1.2. How collective effects influence the bubble velocity. All experiments reveal that the mean rise velocity $\langle V \rangle$ of the bubbles in a homogeneous bubble swarm is lower than that determined in the case of an isolated bubble [by about 30% at $\alpha = 15\%$ (Colombet et al. 2015)]. Its value has been found to be a decreasing function of the gas volume fraction for a wide range of α ($0.5\% \lesssim \alpha \lesssim 35\%$) and Re ($10 \lesssim Re \lesssim 1,000$) in experiments (Zenit et al. 2001, Garnier et al. 2002, Martínez Mercado et al. 2007, Roig & de Tournemine 2007, Riboux et al. 2010, Colombet et al. 2015), as well as in DNS (Roghair et al. 2013). The decrease of $\langle V \rangle$ is generally attributed to a hindrance effect resulting from the counterflow generated between the bubbles in order to balance

the flow entrained in the vicinity of each bubble. Even though several empirical correlations have been proposed (Roghair et al. 2011a, 2013), so far no theory exists to predict the evolution of $\langle V \rangle$ with α.

Whereas measurements of the average bubble velocity are rather robust, determining the bubble velocity fluctuations is tricky. At very low gas volume fraction ($\alpha \leq 1\%$), accurate measurements of bubble velocity fluctuations have been achieved by means of particle-tracking velocimetry (PTV) (Martínez Mercado et al. 2010). PTV can be additionally used at larger gas volume fractions ($\alpha \leq 15\%$), but in this case, it will be limited to measurements performed in the vicinity of a wall (Colombet et al. 2015). Experiments conducted at large Re and low α show that horizontal fluctuations are much more intense than vertical ones and that their probability density functions (PDFs) follow a non-Gaussian distribution with exponential tails. These fluctuations are dominated by wake-induced path oscillations and are similar to those of an isolated bubble. A double optical probe is commonly used to address a large range of gas volume fractions. It records the propagation time τ_{op} of the bubble interfaces between two points separated by a distance δ_{op} in the vertical direction (Kiambi et al. 2003). Dividing δ_{op} by τ_{op} gives a velocity sample v_{op}. For a bubble of constant shape and orientation rising on a straight vertical path, v_{op} corresponds to the vertical component of the bubble velocity. For a deformed bubble following an oscillatory path, v_{op} also includes contributions of the horizontal component of the velocity as well as the rotation rate. Even though v_{op} is not perfectly defined, its standard deviation v'_{op} can be used to characterize the global agitation of the bubbles. Surprisingly, v'_{op} is observed to be almost independent of α when $0 \leq \alpha \lesssim 35\%$ and $50 \lesssim Re \lesssim 1,000$ (Martínez Mercado et al. 2007, Riboux et al. 2010, Colombet et al. 2015).

On the one hand, the average bubble velocity depends on the gas volume fraction and is sensitive to local inhomogeneities of the bubble distribution. On the other hand, the intensity of the bubble agitation remains mainly controlled by wake-induced path oscillations and is rather independent of bubble interactions, even at significant gas volume fractions.

3.2. Liquid Dynamics

We now address the dynamics of the liquid phase by considering the energy, the PDFs, and the spectra of the velocity fluctuations.

3.2.1. Energy of liquid fluctuations. At variance with bubbles, the agitation of the liquid regularly increases with the gas volume fraction, regardless of the values of the Reynolds or the Weber number (Martínez Mercado et al. 2007). For $Re \geq O(100)$, the variance of the liquid velocity normalized by the square of the bubble rise velocity is observed to be roughly proportional to the gas volume fraction: $\langle u^2 \rangle / \langle V \rangle^2 = \kappa \alpha$, where the proportionality coefficient κ is a decreasing function of Re. In this expression, the average bubble velocity $\langle V \rangle$ is a function of α. It is therefore interesting to investigate how $\langle u^2 \rangle$ scales with the velocity of an isolated bubble $\langle V_0 \rangle$, which corresponds to the limit case where $\alpha = 0$. In agreement with the observations of Risso & Ellingsen (2002), various experiments (Martínez Mercado et al. 2007, Roig & de Tournemine 2007, Riboux et al. 2010) pointed out that the standard deviations of the vertical and horizontal liquid velocities are well described by the following expressions:

$$\langle u_x^2 \rangle^{1/2} = \gamma_x \langle V_0 \rangle \alpha^{0.4}, \qquad\qquad 1.$$

$$\langle u_z^2 \rangle^{1/2} = \gamma_z \langle V_0 \rangle \alpha^{0.4}. \qquad\qquad 2.$$

A linear superposition of the disturbances generated by the bubbles should lead to a linear dependence of the fluctuating energy with α. The actual evolution of the energy as α^n with a value

of $n \approx 0.8$ significantly smaller than unity is attributed to nonlinear interactions between bubbles, which may enhance the energy dissipation. From the work of Lance & Bataille (1991), many studies confirmed that the energy of vertical fluctuations is larger than that of horizontal ones: $\gamma_z = 1.14$ and $\gamma_x = 0.76$ for the case of a bubble of $d = 2.1$ mm rising in water ($\langle V_0 \rangle = 320$ mm s^{-1}) (Riboux et al. 2010).

It is important to mention that variance measurements only give a rough description of liquid fluctuations. First, it is difficult to assess their accuracy because the variance depends significantly on the largest velocity fluctuations that are localized in the vicinity of the interfaces, where spurious measurements and lack of detections are common. Second, the variance only describes a small part of the statistical information when the fluctuations do not follow a Gaussian distribution.

3.2.2. Probability density functions of liquid fluctuations. PDFs of BIA have been reported in several experimental works (Zenit et al. 2001; Risso & Ellingsen 2002; Rensen et al. 2005; Martínez Mercado et al. 2007, 2010; Riboux et al. 2010, Prakash et al. 2016). **Figure 4** represents a typical example of PDFs of the vertical and horizontal liquid fluctuations measured in a homogeneous bubble swarm. The velocities have been normalized by the standard deviation of the fluctuations in the corresponding direction to facilitate the comparison between the various gas volume fractions. A semilogarithmic scale is used so that a linear evolution on the graph represents exponential behavior.

The vertical PDFs are clearly non-Gaussian. First, they are strongly asymmetric, with large positive (upward) fluctuations more probable than large negative (downward) ones. Second, they can be described as a succession of decreasing exponential evolutions, $\exp(-\beta \, |u_i|)$, of different slopes β. Positive fluctuations show a first rapid exponential decay with a large slope followed by
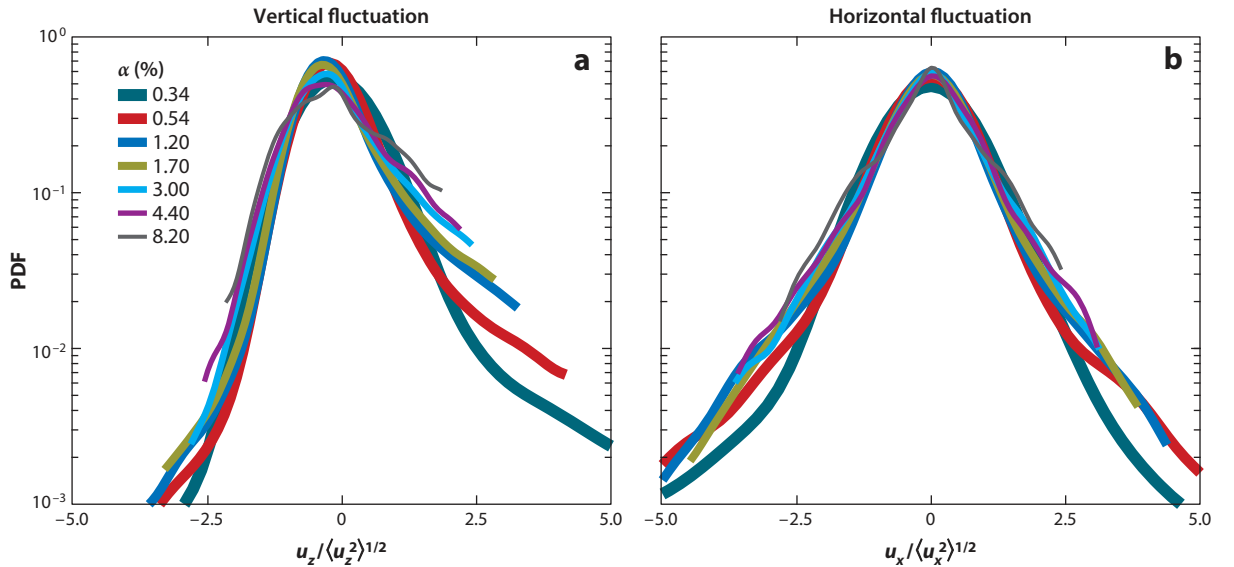

Figure 4

Probability density functions of bubble-induced liquid fluctuations in (*a*) vertical and (*b*) horizontal velocities. Data taken from Riboux et al. (2010). Abbreviations: α, gas volume fraction; PDF, probability density function.

a slower exponential decay with a smaller slope at large fluctuations. Negative fluctuations show similar behavior but the slower decay concerns only very rare events. Except for the fact that they are symmetric, horizontal PDFs resemble vertical ones, with high exponential decreases for small fluctuations followed by gentle ones at large fluctuations. When α varies, the central part of both the horizontal and vertical PDFs remains almost unchanged, whereas the exponential tails corresponding to large fluctuations are modified, as well as the velocity at which the transition between the two different slopes occurs. This indicates that the small and large velocity fluctuations are controlled by different mechanisms involving a different scaling.

3.2.3. Spectra, length scales, and timescales.

A comprehensive description of liquid agita-tion requires the specification of the characteristic time and length scales of the flow. This information is generally obtained from the average spectra of the fluctuations, which are usually determined by taking the Fourier transform of a velocity signal. In bubbly flows, velocity signals are discontinuous, however, because of the interruptions by the bubble interfaces. There is therefore no straightforward definition of the velocity spectrum of bubble-induced liquid velocity fluctuations. Different approaches have been used to deal with a continuous signal: filling the gaps by a smooth Gaussian function (Lance & Bataille 1991), considering only intervals between bubbles where the signal is continuous (Martínez Mercado et al. 2010, Roghair et al. 2011b, Mendez-Diaz et al. 2013, Prakash et al. 2016), or investigating the flow just behind a rising swarm of bubbles (Riboux et al. 2010). Moreover, depending on the configuration and measurement technique, the considered velocity signals differ from one another in the different investigations. Most of the time, an average frequency spectrum is determined from the time series of liquid velocity samples that are acquired at a single point: Sometimes the probe is fixed and no mean liquid velocity is present (Martínez Mercado et al. 2010, Roghair et al. 2011b); other times, a uniform mean liquid velocity is imposed (Lance & Bataille 1991) or the probe is moved at constant velocity in the horizontal direction (Mendez-Diaz et al. 2013). Riboux et al. (2010) computed wave number spectra from spatial series of velocity samples regularly distributed on a line, which were obtained by PIV. If the Eulerian length scales that are obtained from a spatial spectrum are unambiguous, the interpretation of the timescales derived from frequency spectra is not evident and depends on the relative motion of the probes with respect to the liquid and the bubbles.

Nevertheless, two properties turn out to be independent of the method used to determine the spectra. First, all experiments considering homogeneous bubble swarms observe a subrange where the power spectral density evolves as the -3 power of either the frequency f or the wave number k, for Reynolds numbers from a few tens to more than 1,000 and for Weber numbers on the order of 1 to 4. It is also found in DNS (Roghair et al. 2011b) or in large-eddy simulation (LES) in which the bubbles wakes are resolved (Riboux et al. 2013), but not in simulations where the bubbles are treated as point particles (Mazzitelli & Lohse 2009), which indicates that this peculiar spectral behavior is related to the existence of wakes behind the bubbles. Second, when normalized by the variance of the fluctuations, the power spectral density becomes independent of the gas volume fraction (Lance & Bataille 1991; Riboux et al. 2010, 2013; Mendez-Diaz et al. 2013). This means that, whereas the energy of the fluctuations increases with α, the characteristic scales of the flow do not depend on α.

Figure 5 shows the evolution of the normalized longitudinal spectra of the vertical, $S_{zz}/\langle u_z^2 \rangle$, and horizontal, $S_{xx}/\langle u_x^2 \rangle$, liquid velocity fluctuations as a function of the reciprocal of the wavelength $\lambda = 2\pi/k$, measured in a homogeneous swarm of 2.5-mm-diameter bubbles rising in water. There are no significant differences between the vertical and the horizontal directions, and the invariance of the normalized spectra with respect to α is observed for the whole available range
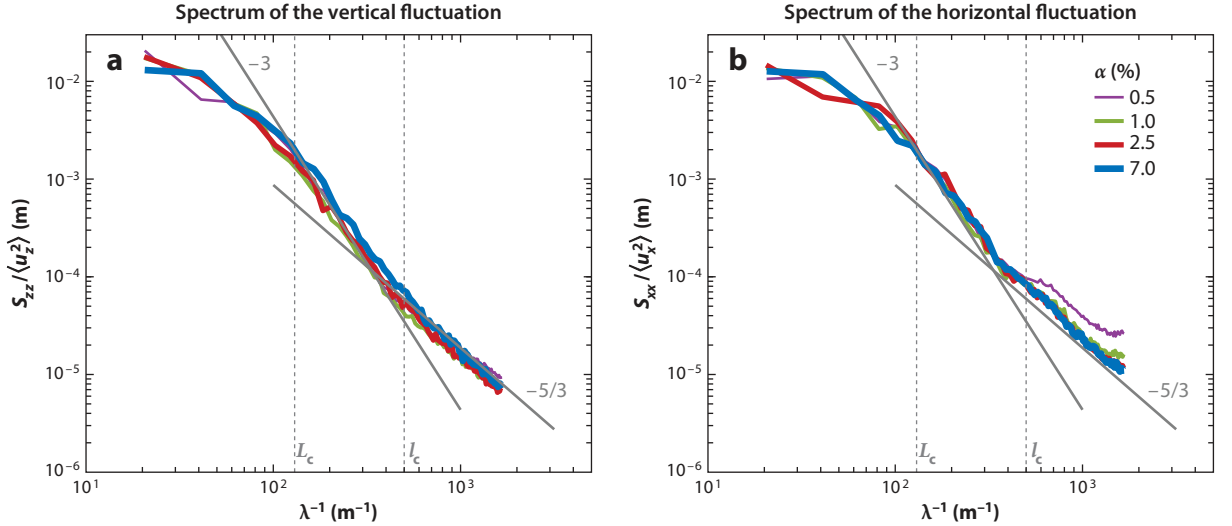
Figure 5

Spectra of bubble-induced liquid fluctuations in (*a*) vertical and (*b*) horizontal velocities. Data taken from Riboux et al. (2010). The limits L_c and l_c of the k^{-3} subrange are indicated by vertical dashed lines. Gray lines show the -3 and $-5/3$ slopes.

of wavelengths. The k^{-3} subrange is observed for the wavelengths between $l_c = 2$ mm and $L_c = 7.7$ mm. It is followed at smaller scales by a $k^{-5/3}$ subrange, which is probably the signature of a classic turbulent inertial subrange. The final dissipative range, which is expected to depend on α, is not observed because the measurement resolution is not sufficient.

Having established the structure of the spectra, it remains to establish their characteristic length scales: the Eulerian integral length scale Λ, the limits L_c and l_c of the k^{-3} subrange for the large scales, and the Kolmogorov scale for the final dissipative range. The two scales that immediately come to mind when seeking the characteristic lengths of a homogeneous bubble swarm are the bubble diameter d and the average distance between the bubbles $(\pi/6\alpha)^{1/3}d$. The average distance is clearly not compatible with the invariance with respect to α. Concerning the bubble diameter, Riboux et al. (2010) did not find any significant difference between the spectra measured for $d = 1.6$, 2.1, and 2.5 mm. They also remarked that the ratio between the bubble diameter and the drag coefficient of a single rising bubble was almost constant for the three diameters they considered: $d/C_d \approx L_c \approx \Lambda/2$. Because it was also found to be related to the length of the bubble wake (see Section 2.2) and consistent with the experiments of Lance & Bataille (1991) where $d = 5$ mm, d/C_d appeared to be a good candidate for the role of the characteristic length scale. However, by considering a much larger range of Re and We, Mendez-Diaz et al. (2013) questioned the relevance of d/C_d for the characterization of the large scales generated by BIA, especially for $Re < 500$.

The dissipative scales are in general below the resolution of the experimental techniques implemented in bubbly flows. But even if the corresponding spectral range is not available, the rate of dissipation of the energy in a steadily rising bubble swarm is equal to the power of the buoyancy force and can thus be determined from the relation $\epsilon = \alpha g \langle V \rangle$. It can also be measured from the decay of the kinetic energy of the liquid fluctuations after the passage of a bubble swarm (Riboux et al. 2010). Then the Kolmogorov microscale η can be estimated from the classic relation for

isotropic turbulence, $\eta = (\nu^3/\epsilon)^{1/4}$. For the case shown in **Figure 5**, η is found to decrease from 0.2 to 0.1 mm when α increases from 4.6% to 12%, evolving broadly as $\alpha^{-0.6}$.

4. PHYSICAL MECHANISMS OF BUBBLE-INDUCED AGITATION

4.1. The Two Causes of Bubble-Induced Agitation

Even if BIA represents only one element of the general picture of a bubbly flow (**Figure 1**), it still involves two different contributions. The first one results from the flow disturbances generated in the vicinity of each bubble. The second one results from the turbulence that develops when the flow through the swarm of bubbles becomes unstable beyond a certain Reynolds number. The different natures of these two contributions are easily understood by considering the ideal situation where the flow disturbance induced by each bubble is steady and all bubbles are moving at the same velocity. In a frame moving with the bubbles, the flow disturbances around the bubbles generate random spatial variations but, contrary to turbulence, do not induce any temporal fluctuations. It is only in the laboratory frame that both contributions generate temporal fluctuations. In practice, bubble velocities fluctuate and it is not possible to define a frame where the bubbles are fixed. Because they involve different mechanisms, the distinction between these two kinds of fluctuations is nevertheless required in order to understand and model high-*Re* BIA.

A few configurations make it possible to distinguish between the fluctuations induced by local bubble disturbances and real turbulence. Bouche et al. (2012, 2014) investigated a homogeneous swarm of quasi-two-dimensional (2D) bubbles confined in a Hele–Shaw cell whose gap (1 mm) was much thinner than the bubble size (≈ 4 mm). The flow regime ($Re \approx 500$) corresponds to ellipsoidal bubbles rising on oscillatory trajectories, and the flow disturbance around each bubble resembles that observed in an unconfined bubble swarm (potential flow above and next to the bubble and an exponentially decaying wake behind it), although the cause of the exponential decrease was the friction at the walls (Roig et al. 2012) rather than interactions between the wakes of neighboring bubbles. Because turbulence cannot develop in such a confined geometry, this configuration is an example of bubbly flow where BIA only results from individual bubble disturbances. Confined bubbly flows are not a good model of 3D ones: Bubble interactions are much stronger in two dimensions, and statistics of both the bubble and liquid velocities evolve differently with the gas volume fraction. However, their PDFs show exponential tails and their spectra exhibit a k^{-3} subrange, indicating that these two properties can be observed in the absence of turbulent fluctuations.

Consider now a steady uniform flow that goes through a random swarm of fixed bubbles with a homogeneous spatial distribution. The velocity fluctuations, $\mathbf{u}(\mathbf{x}, t) = \mathbf{U}(\mathbf{x}, t) - \langle \mathbf{U} \rangle$, can be decomposed by the combined use of spatial averaging, denoted by angle brackets, and time averaging, denoted by an overbar (Risso et al. 2008):

$$\mathbf{u}(\mathbf{x}, t) = \overline{\mathbf{u}}(\mathbf{x}) + \mathbf{u}'(\mathbf{x}, t). \qquad 3.$$

On the one hand, the spatial fluctuation $\overline{\mathbf{u}}(\mathbf{x})$, which only depends on the spatial coordinate $\mathbf{x}$, corresponds to the contribution of the individual bubble disturbances. On the other hand, the temporal fluctuation $\mathbf{u}'(\mathbf{x}, t)$, which still depends on both the time t and the location $\mathbf{x}$, accounts for the turbulence. The variances of the total fluctuation $\mathbf{u}(\mathbf{x}, t)$ are the sum of the variances of these two contributions:

$$\langle \mathbf{u}^2 \rangle = \langle \overline{\mathbf{u}}^2 \rangle + \langle \mathbf{u}'^2 \rangle. \qquad 4.$$

Total fluctuation
$u_z(\mathbf{x}, t)/\langle V \rangle$

Spatial fluctuation
$\overline{u_z}(\mathbf{x})/\langle V \rangle$

Time fluctuation
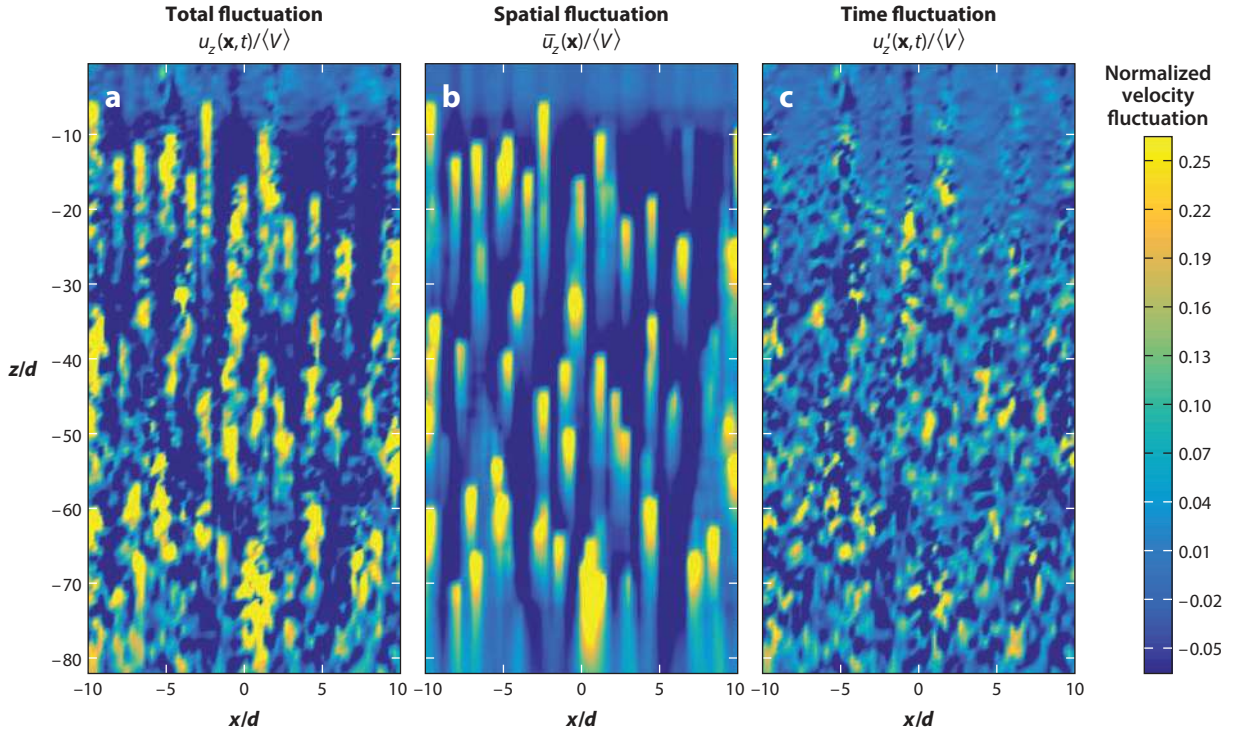$u'_z(\mathbf{x}, t)/\langle V \rangle$

Figure 6

Fields of vertical velocity in a vertical plane computed by large-eddy simulation (Riboux et al. 2013). The total fluctuation (*a*), $u_z(\mathbf{x}, t) = \overline{u_z}(\mathbf{x}) + u'_z(\mathbf{x}, t)$, has been decomposed into its (*b*) spatial fluctuation $\overline{u_z}(\mathbf{x})$ and (*c*) temporal fluctuation $u'_z(\mathbf{x}, t)$ components.

Riboux et al. (2013) first investigated by means of LES the flow of water through a random swarm of air bubbles (**Figure 6**). Each bubble was modeled as a fixed source of momentum that was distributed over a few mesh sizes. Because the grid spacing was of the order of the bubble diameter, scales smaller than a bubble were not resolved, and the simulated flow therefore essentially resulted from large-scale interactions between the bubble wakes. In addition, the flow through a random array of fixed solid spheres was investigated experimentally (Amoura 2008, Risso et al. 2008, Amoura et al. 2017).

Figures 7 and **8** show the PDFs and the spectra of the total spatial and temporal fluctuations computed by LES or measured in a random array of spheres, as well as the total fluctuation measured in a real bubble swarm. It is worth mentioning that the ratios of the vertical to the horizontal total fluctuations differ according to the configuration: $\sqrt{\langle u_z^2 \rangle / \langle u_x^2 \rangle} \approx 1.5$ in the real bubble swarm, 2.4 in the array of spheres, and 3 in the LES. Oscillatory motions of the bubbles are responsible for a more efficient energy redistribution between the velocity components, which probably explains the larger anisotropy observed for fixed bubbles or spheres. In **Figure 7**, each velocity fluctuation has been normalized by the standard deviation of the total fluctuation of the corresponding velocity component, in order to improve comparisons of the PDF shape in the different situations. In **Figure 8**, the spectrum of each contribution has been normalized by using its own variance and the integral length scale of the temporal fluctuation. Given the coarse resolution of the LES and the differences between solid spheres and bubbles, the PDFs and the spectra of the normalized total fluctuations in the two idealized flows are in remarkable agreement
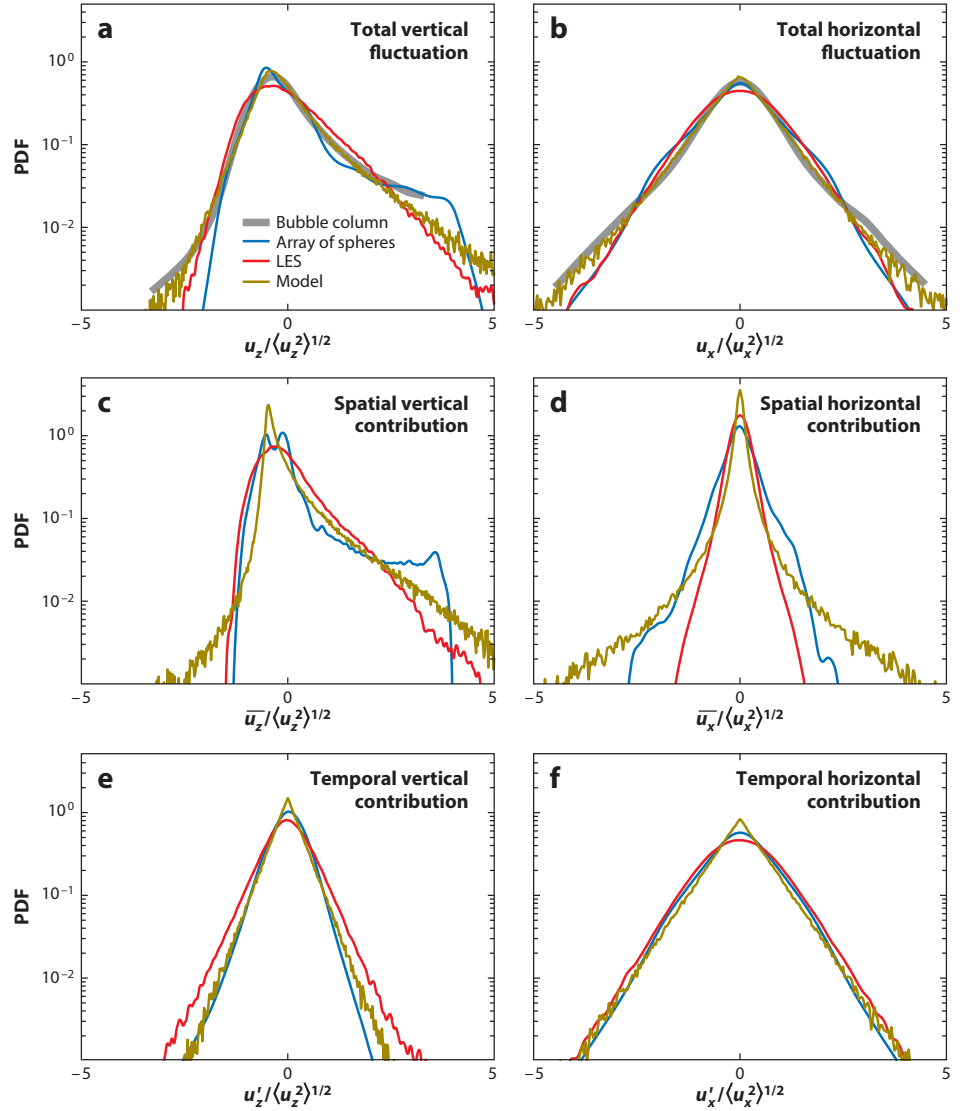
Figure 7

Probability density functions of bubble-induced liquid fluctuations decomposed into their different contributions. Red lines indicate large-eddy simulation (LES) ($\alpha = 1.9$, $Re = 760$) from Riboux et al. (2013); blue lines indicate random array of spheres ($\alpha = 2.0$, $Re = 1,000$) from Amoura (2008) and Amoura et al. (2017); thick gray lines indicate measurements in a real bubble swarm ($\alpha = 1.7$, $Re = 760$) from Riboux et al. (2010); yellow lines indicate the model from Risso (2016). Abbreviations: α, gas volume fraction; PDF, probability density function.

with those of a real bubble swarm. Whereas the energy of the fluctuations depends on the nature of the dispersed phase and on the fluctuating motions of the bubbles, the structure of the fluctuations mainly results from large-scale interactions between wakes.

Let us distinguish now the contributions of the spatial and temporal fluctuations. The PDF of the spatial fluctuation in the vertical direction is dominated by a long tail corresponding to
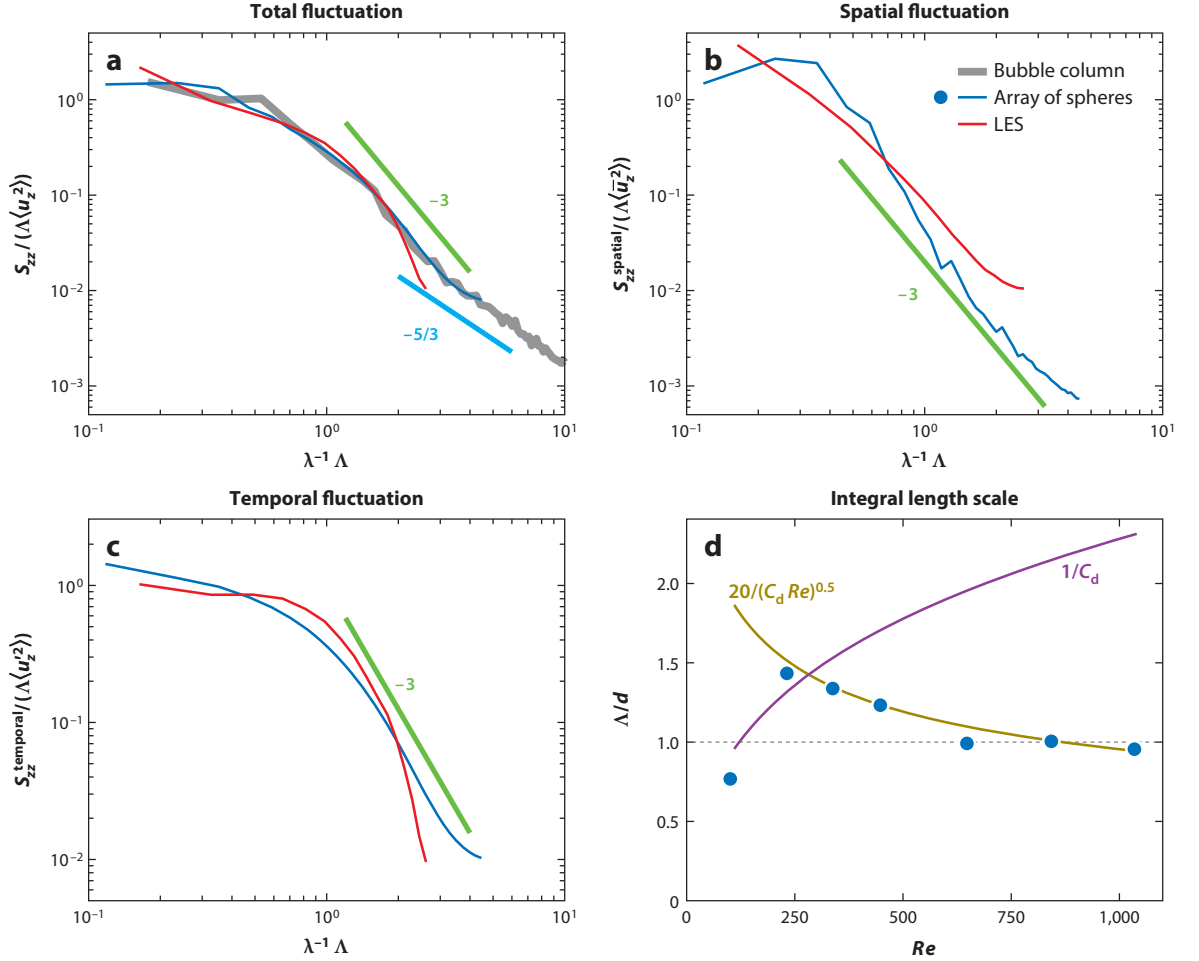
Figure 8

(*a–c*) Normalized spectra of bubble-induced liquid fluctuations decomposed into their different contributions. Red lines indicate large-eddy simulation (LES) ($\alpha = 1.9$, $Re = 760$) from Riboux et al. (2013); blue lines indicate random array of spheres ($\alpha = 2.0$, $Re = 1{,}000$) from Amoura (2008) and Amoura et al. (2017); the thick gray line indicates measurements in a real bubble swarm ($\alpha = 1.7$, $Re = 760$) from Riboux et al. (2010). (*d*) Evolution of the Eulerian integral length scale as a function of the Reynolds number measured in a random array of spheres.

large upward fluctuations. The PDF of the horizontal spatial fluctuation and the PDFs of the temporal fluctuation in both directions are symmetric and well described by an exponential law, $\exp(-\beta\,|\,u_i\,|)$. The temporal fluctuations are isotropic and have a slope β larger than that of the horizontal spatial fluctuation. In the vertical direction, the total fluctuation is dominated by the temporal contribution at moderate fluctuations and by the spatial contribution at large positive fluctuations. In the horizontal direction, the total fluctuation is dominated by the temporal contribution at moderate fluctuations and by the spatial contribution at large fluctuations. As can be seen in **Figure 4**, the spatial contribution starts to dominate the PDFs for increasingly lower velocity fluctuations as the gas volume fraction increases. The succession of exponential decays with different slopes in the PDFs of the total fluctuation therefore results from the combination of

the spatial and temporal fluctuations. Regarding the spectra, the spatial contribution dominates at large scales, whereas the temporal contribution dominates at small scales, but both contributions generate a k^{-3} subrange.

4.2. Interpretation and Modeling

Thanks to investigations of the flow through a random array of obstacles, the main features of the PDFs and the spectra of the total fluctuations have been attributed either to individual bubble disturbances (spatial fluctuations) or to fluctuations resulting from the flow instability (temporal fluctuations). We discuss now the underlying mechanisms.

4.2.1. Flow disturbances generated by the bubbles. The simplest way to model the fluctuations induced by individual bubble disturbances is to linearly superimpose them. The bubbles are randomly distributed over space and their positions are assumed to be independent of each other. Then, the liquid velocity at a given point is computed as the sum of the flow disturbances generated by each bubble. This requires a realistic model of the flow around a bubble. Such an approach was first implemented by considering the potential flow around a bubble (Biesheuvel & van Wijngaarden 1984, Lance & Bataille 1991) and the wake of an isolated bubble, which was truncated to avoid the divergence of the energy (Parthasarathy & Faeth 1990). As seen in Section 2.2, the flow around a bubble immersed in a bubble swarm is potential above and next to the bubble, but involves a wake that is exponentially attenuated by interaction with the wakes of the neighboring bubbles and is almost constant for $\alpha = 0.5$–10%. Risso (2016) considered the sum of (*a*) the potential flow around a spheroidal bubble of aspect ratio ξ and (*b*) a vertical disturbance generated by a Gaussian wake that exponentially decays with the vertical distance to the bubble: $u_z = \exp(-z/L)\exp\left(-(x^2 + y^2)/w^2\right)$, where L and w are the characteristic length and width of the wake, respectively. The PDFs of the fluctuations were then computed from samples of randomly chosen bubble locations. Given d, ξ, $\langle V \rangle$, an d α, it turns out that the PDFs only depend on the wake volume Lw^2, which can be fitted on the experimental PDFs of the total fluctuation measured in a homogeneous bubble swarm by considering the large positive vertical fluctuations, which have been shown to be controlled by the spatial fluctuation. In practice, the value of Lw^2 is independent of α but is obtained with better accuracy for a gas volume fraction around 4% at which the spatial fluctuations are probable enough. **Figure 7*c*,*d*** shows the PDFs computed with this model together with the PDFs of the spatial fluctuations computed by LES or measured in an array of spheres. In the vertical direction, large positive fluctuations are dominated by the bubble wakes, whereas rare large negative fluctuations are due to the potential flow. In the horizontal direction, the wake contribution is negligible and the exponential tails are due to the potential contribution.

We can also wonder what the spectral signature of a population of velocity disturbances randomly distributed over space is. Considering that the disturbances have a smooth pattern, that their magnitude and size are statistically independent, and that their size is uniformly distributed between two finite lengths L_{min} and L_{max}, it has been demonstrated that the spatial spectrum follows a k^{-3} law for wavelengths in the range from L_{min} to L_{max} (Risso 2011).

The main features of the PDFs and the spectra of the spatial fluctuations can thus be reproduced by the linear superimposition of independent individual disturbances.

4.2.2. Turbulence induced by the bubbles. Having regarded the properties of the temporal fluctuations in a flow through a random array of fixed obstacles, Risso (2016) proposed to describe the PDF of the turbulent contribution to the fluctuations in a real bubble swarm by an exponential

function:

$$f_t(u') = \frac{\sqrt{2}}{2\sigma_t} \exp\left(-\frac{\sqrt{2}\,|u'|}{\sigma_t}\right),$$

5.

where $\sigma_t = (\alpha/0.01)^{0.4} v_t$. Assuming that bubble-induced turbulence is isotropic, Equation 5 is used for all the velocity components with the same standard deviation σ_t. The value of v_t can be deduced from the slope β of the first exponential decay of the horizontal total fluctuations at low α, which has been shown to be dominated by the temporal fluctuation. **Figure 7e,f** shows these model PDFs for a value of v_t that has been measured from experimental total fluctuations at $\alpha = 0.34\%$. They reasonably collapse with the temporal fluctuations computed from LES with bubbles or measured in experiments with fixed solid spheres.

The interest of this model is to extract the turbulent contribution from the total fluctuation measured in real bubble experiments. However, it cannot help us much to interpret the mechanisms of bubble-induced turbulence and the reason for the exponential PDFs and k^{-3} spectral subrange. LES of the flow through a population of fixed bubbles (Riboux et al. 2013) provides some additional clues. First, whereas the flow that is computed by considering a single bubble remains stationary, the flow that is computed with a population of bubbles reveals temporal fluctuations. Second, significant fluctuations are not localized in the bubble wakes but rather are distributed in a homogeneous way across space (**Figure 6**). Third, the average frequency spectrum of the fluctuations, which is obtained from a Fourier transform of the time evolutions of the liquid velocity at a given position, shows that the energy density is concentrated around a frequency $f_c = 0.14\langle V \rangle/d$. At low α and moderate Re, the spectrum presents a sharp peak at f_c, which broadens when the energy of the fluctuations is increased by increasing either α or Re. The authors conclude that temporal fluctuations are the result of a collective instability of the flow involving nonlinear interactions between bubble wakes.

Lance & Bataille (1991) considered the energy balance in the spectral space. In a statistically steady and homogeneous state, the power spectral density E of the turbulent fluctuations is related to the energy production Π and to the energy transfer T between the wave numbers by

$$2\nu k^2 E = T + \Pi.$$

6.

They considered that the turbulent fluctuations were localized within the bubble wakes where they were both produced and dissipated. Assuming that the production only depends on the dissipation rate ϵ and on the wave number k, dimensional considerations lead to $\Pi \propto \epsilon k^{-1}$. Inserting this expression into Equation 6 and neglecting T, they obtained a spectrum in k^{-3}:

$$E \propto \frac{\epsilon k^{-3}}{2\nu}.$$

7.

Due to the results of LES in which the scales smaller than the wakes are not resolved (Riboux et al. 2013) and to the fact that a k^{-3} subrange has been observed in experiments for scales larger than d (Riboux et al. 2010), the assumption that turbulence is localized within the wakes is invalidated. However, the assumption that Π and T depend only on ϵ and k is less restrictive and still leads to Equation 7.

Now, recall that the spectrum is invariant with respect to α when normalized by the variance $\langle u'^2 \rangle$ of the fluctuation and the integral length scale Λ. In particular, this implies the following relation for the k^{-3} subrange:

$$\frac{E}{\langle u'^2 \rangle \Lambda} \propto (\Lambda k)^{-3}.$$

8.

Equating Equations 7 and 8 yields

$$\epsilon \propto \frac{\nu \langle u'^2 \rangle}{\Lambda^2}, \qquad\qquad 9.$$

where Λ appears as a kind of Taylor scale for the k^{-3} subrange. Taking into account that $\epsilon = \alpha g \langle V \rangle$ and $\langle u'^2 \rangle \propto \alpha \langle V \rangle^2$ finally leads to the following scaling for Λ:

$$\Lambda \propto \sqrt{\frac{\nu \langle V \rangle}{g}} \propto \frac{d}{\sqrt{C_d Re}}. \qquad\qquad 10.$$

The interest of this relation is that it can be tested in experiments or simulations to assess the validity of the assumptions leading to Equation 7. For the experiments of Riboux et al. (2010), taking the values of Re and C_d corresponding to an isolated bubble, Equation 10 leads to the same value of Λ for the three investigated bubble diameters, which is in agreement with the observations. Note that for these particular bubble sizes, C_d was almost proportional to Re, which explains why the scaling $\Lambda \propto d/C_d$ proposed by the authors was also in agreement with the experiments. In **Figure 8d**, the various scalings for Λ have been compared to the results obtained in an random array of fixed spheres for various Re by estimating C_d by the Schiller and Naumann relation for an isolated solid sphere. It turns out that Equation 10 gives the correct evolution of Λ, whereas d or d/C_d do not. Comparisons with other investigations covering a broader range of parameters are nevertheless required to reach a definitive conclusion regarding the validity of Equations 7 and 10.

4.2.3. Total fluctuation. Distinguishing the contribution of individual bubble disturbances from that of turbulence proved useful so far. However, the question of how they combine together to constitute the total BIA remains.

Risso (2016) assumed that a fluctuation sample at given instant and location was the sum of the contribution of individual bubble disturbances and of that of turbulent fluctuations. The first contribution was computed by considering a random distribution of the bubbles around the measurement point. The second was computed by randomly choosing a realization of a random variable following the probability density defined by Equation 5. Assuming that both contributions were statistically independent, a statistically representative ensemble of samples of total fluctuations was obtained. The PDFs were compared to experimental results by independently adjusting the values of the wake volume Lw^2 and of the reference turbulent velocity v_t, as described in Sections 4.2.1 and 4.2.2. **Figure 7a,b** shows the model PDFs for $\alpha = 1.7\%$. The model turned out to describe well the evolution with the gas volume fraction of the experimental PDFs for $\alpha = 0.3–8\%$ without any further parameter adjustment. Therefore, it can be used to estimate the relative contribution of each kind of fluctuation in a real bubbly flow. It is worth noting that the assumption of statistical independence of the two contributions is in conflict with turbulent fluctuations localized within bubble wakes. However, it is compatible with turbulent fluctuations resulting from the interactions between the bubble wakes. It is also consistent with the fact that significant temporal fluctuations were found outside the wake in LES results (**Figure 6c**).

With regard to the spectra, both contributions follow a k^{-3} power law in the range of wavelengths where they are likely to have comparable intensity. This is probably the reason why a k^{-3} subrange is observed for such a wide range of Reynolds numbers. But it does not provide any clues about a possible interaction between the two contributions.

5. CONCLUDING REMARKS AND PROSPECTS

The statistical properties of the agitation induced by a homogeneous swarm of bubbles rising at large Reynolds number ($Re \geq 100$) are now rather well known.

The average velocity of the bubbles within a bubble swarm is lower than that of an isolated bubble and decreases as the gas volume fraction increases. This phenomenon is attributed to a hindrance mechanism caused by the return flow required to balance the flow entrainment by the bubbles. From a theoretical point of view, it is not well understood and presently no universal model has been developed to describe it. The wake of a bubble is usually unstable because of the interface deformation or the presence of surface-active contaminants. The bubble velocity fluctuations are generally dominated by wake-induced path oscillations, and their variance is weakly dependent on the gas volume fraction.

In contrast, the variance of the liquid velocity fluctuations increases almost proportionally to the gas volume fraction. BIA involves two kinds of fluctuations. The first one results from the flow disturbance induced by each bubble, which weakly depends on α, and it involves both a potential contribution and a strongly attenuated wake. It is the main cause of anisotropy and generates the fluctuations with the greatest intensity and of the largest scales. It is responsible for the exponential tails on the sides of the PDFs and produces a k^{-3} spectral subrange. The second kind of fluctuation is the turbulence that results from the instability of the whole flow. It is almost isotropic and weakly correlated to the bubble positions. It is responsible for the central exponential parts of the PDFs and also generates a k^{-3} spectral subrange. It is worth noting that all of these characteristics are rather independent of the exact nature of the dispersed phase (solid spheres or bubbles) and of whether the bubbles are moving relatively to each other or not. This is not the case for the variance of the fluctuations and the ratio of anisotropy, which depend on the precise details of the configuration. Whereas the fluctuations induced by individual bubble disturbances are now well understood, the mechanism driving the turbulence production still needs to be elucidated. A first direction for future research is to achieve a definitive determination of the characteristic scale of the k^{-3} subrange, wherein energy is continuously injected by the bubbles. Another promising direction is the numerical investigation of a random array of interacting wakes: in particular, the study of the flow stability and the analysis of the energy budget in the spectral domain.

Two other issues that are important both from a fundamental point of view and for applications are how BIA mixes up a tracer and how it influences interfacial mass transfer. Alméras et al. (2015) experimentally investigated the mixing of a low-diffusive dye in a homogeneous swarm of air bubbles ($d = 2.1$ mm) rising in water. It turns out that, at a scale of few bubble diameters, it can be described by an anisotropic regular diffusion process, with a more efficient diffusion in the vertical direction than in the horizontal one. The diffusion coefficient D_i in direction i was found to be the product of the variance of the fluctuations in the considered direction and of a timescale T_D: $D_i = \langle u_i^2 \rangle T_D$. At low gas volume fraction, T_D corresponds to the correlation time of the BIA ($T_D \propto \Lambda / \langle u_i^2 \rangle^{1/2}$) and D_i increases as $\alpha^{1/2}$. At larger α, T_D is given by the time interval between two consecutive bubbles at a given location, and D_i converges towards a value independent of α. It thus appears that the mixing can be related to the characteristics of the BIA. Colombet et al. (2015) investigated the mass transfer between the bubbles and the liquid in a similar configuration where the concentration of dissolved gas was homogeneous in the whole flow. Under these conditions, the transfer mainly occurs at the front of the bubbles where the mean flow is potential. Moreover, the smallest scales of the BIA are much larger than the thickness of the diffusion layer at the bubble interface. For these reasons, the rate of mass transfer is unaffected by the BIA and remains close to the value corresponding to a single rising bubble, up to a gas volume fraction of 30%. Future research should address the cases where large-scale mixing and mass transfer occur simultaneously.

The next important challenge is to understand how BIA interacts with SIT. A first promising way is the one highlighted by Prakash et al. (2016). It consists of injecting a homogeneous bubble swarm into grid-generated turbulence. It has already been shown how the specific properties of BIA, such as the exponential tails of PDFs, emerge when the ratio between the intensity of BIA

and that of SIT is increased. Future research should consider varying the integral length scale of SIT relative to that of BIA in order to change the overlap between the k^{-3} subrange of BIA and the $k^{-5/3}$ inertial subrange of SIT. Varying both the relative intensity and length scales is probably a relevant method to reveal the coupling between the two sources of fluctuations. A second important phenomenon is the interaction between BIA and buoyancy-driven flows caused by gradients of the gas volume fraction. This could be investigated by considering a bubble column at the bottom of which we can impose a gas injection gradient (Alméras 2014). At uniform gas injection, the bubble column is stable and homogeneous. From a certain inlet gradient, large-scale circulations are first observed. Then, while the inlet gradient further increases, fluctuations of lower and lower scales develop, eventually leading to a classic turbulent cascade. This configuration should thus make it possible to study of the transition from a situation where the fluctuations resulting from the buoyancy-driven flow only concern scales that are much larger than those of BIA to a situation where the spectra overlap.

DISCLOSURE STATEMENT

The author is not aware of any biases that might be perceived as affecting the objectivity of this review.

LITERATURE CITED

Alméras E. 2014. *Étude des propriétés de transport et de mélange dans les écoulements à bulles*. PhD Thesis, Univ. Toulouse

Alméras E, Risso F, Roig V, Cazin S, Plais C, Augier F. 2015. Mixing by bubble-induced turbulence. *J. Fluid Mech.* 776:458–74

Amoura Z. 2008. *Étude hydrodynamique de l'écoulement traversant un réseau aléatoire de sphères fixes*. PhD Thesis, Univ. Toulouse

Amoura Z, Besnaci C, Risso F, Roig V. 2017. Velocity fluctuations generated by the flow through a random array of spheres: a model of bubble-induced agitation. *J. Fluid Mech.* 823:592–616

Aybers NM, Tapucu A. 1969. The motion of gas bubbles rising through stagnant liquid. *Wärme Stoffübertrag.* 2:118–28

Balachandar S, Eaton JK. 2010. Turbulent dispersed multiphase flow. *Annu. Rev. Fluid Mech.* 42:111–33

Batchelor GK. 1967. *An Introduction to Fluid Dynamics*. Cambridge, UK: Cambridge Univ. Press

Bel Fdhila R, Duineveld PC. 1996. The effect of surfactant on the rise of a spherical bubble at high Reynolds and Peclet numbers. *Phys. Fluids* 8:310–21

Biesheuvel A, van Wijngaarden L. 1984. Two-phase flow equations for a dilute dispersion of gas bubbles in liquid. *J. Fluid Mech.* 148:301–18

Bouche E, Roig V, Risso F, Billet AM. 2012. Homogeneous swarm of high-Reynolds-number bubbles rising within a thin gap. Part 1. Bubble dynamics. *J. Fluid Mech.* 704:211–31

Bouche E, Roig V, Risso F, Billet AM. 2014. Homogeneous swarm of high-Reynolds-number bubbles rising within a thin gap. Part 2. Liquid dynamics. *J. Fluid Mech.* 758:508–21

Brücker C. 1999. Structure and dynamics of the wake of bubbles and its relevance for bubble interaction. *Phys. Fluids* 11:1781–96

Bunner B, Tryggvason G. 2002a. Dynamics of homogeneous bubbly flows. Part 1. Rise velocity and microstructure of the bubbles. *J. Fluid Mech.* 466:17–52

Bunner B, Tryggvason G. 2002b. Dynamics of homogeneous bubbly flows. Part 2. Velocity fluctuations. *J. Fluid Mech.* 466:53–84

Bunner B, Tryggvason G. 2003. Effect of bubble deformation on the properties of bubbly flows. *J. Fluid Mech.* 495:77–118

Caflisch RE, Luke JHC. 1985. Variance in the sedimentation speed of a suspension. *Phys. Fluids* 28:759–53

Cartellier A, Andreotti M, Séchet P. 2009. Induced agitation in homogeneous bubbly flows at moderate particle Reynolds number. *Phys. Rev. E* 80:065301

Cartellier A, Rivière N. 2001. Bubble-induced agitation and microstructure in uniform bubbly flows at small to moderate particle Reynolds numbers. *Phys. Fluids* 13:2165–81

Chahed J, Roig V, Masbernat L. 2003. Eulerian–Eulerian two-fluid model for turbulent gas–liquid bubbly flows. *Int. J. Multiph. Flow* 29:23–49

Climent E, Magnaudet J. 1999. Large-scale simulations of bubble-induced convection in a liquid layer. *Phys. Rev. Lett.* 82:4827–30

Colombet D, Legendre D, Risso F, Cockx A, Guiraud P. 2015. Dynamics and mass transfer of rising bubbles in a homogenous swarm at large gas volume fraction. *J. Fluid Mech.* 763:254–85

Cuenot B, Magnaudet J, Spennato B. 1997. The effects of slightly soluble surfactants on the flow around a spherical bubble. *J. Fluid Mech.* 339:25–53

Duineveld PC. 1995. The rise velocity and shape of bubbles in pure water at high Reynolds number. *J. Fluid Mech.* 292:325–32

Ellingsen K, Risso F. 2001. On the rise of an ellipsoidal bubble in water: oscillatory paths and liquid-induced velocity. *J. Fluid Mech.* 440:235–68

Ern P, Risso F, Fabre D, Magnaudet J. 2012. Wake-induced oscillatory paths of bodies freely rising or falling in fluids. *Annu. Rev. Fluid Mech.* 44:97–121

Esmaeeli A, Tryggvason G. 1999. Direct numerical simulations of bubbly flows. Part 2. Moderate Reynolds number arrays. *J. Fluid Mech.* 385:325–58

Esmaeeli A, Tryggvason G. 2005. A direct numerical simulation study of the buoyant rise of bubbles at $O(100)$ Reynolds number. *Phys. Fluids* 17:093303

Figueroa-Espinoza B, Zenit R. 2005. Clustering in high Re monodispersed bubbly flows. *Phys. Fluids* 17:091701

Ford B, Loth E. 1998. Forces on ellipsoidal bubbles in a turbulent shear layer. *Phys. Fluids* 10:178–88

Garnier C, Lance M, Marié JL. 2002. Measurement of local flow characteristics in buoyancy-driven bubbly flow at high void fraction. *Exp. Therm. Fluid Sci.* 26:811–15

Gatignol R. 1983. The Faxén formulas for a rigid particle in an unsteady non-uniform Stokes flow. *J. Mec. Theor. Appl.* 2:143–60

Hallez Y, Legendre D. 2011. Interaction between two spherical bubbles rising in a viscous liquid. *J. Fluid Mech.* 673:406–31

Harteveld WK. 2005. *Bubble columns: structures or stability?* PhD Thesis, Tech. Univ. Delft

Harteveld WK, Mudde RF. 2003. Dynamics of a bubble column: influence of gas distribution on coherent structures. *Can. J. Chem. Eng.* 81:389–94

Hunt J, Eames I. 2002. The disappearance of laminar and turbulent wakes in complex flows. *J. Fluid Mech.* 457:111–32

Kiambi SL, Duquenne AM, Dupont JB, Colin C, Risso F, Delmas H. 2003. Measurements of bubble characteristics: comparison between double optical probe and imaging. *Can. J. Chem. Eng.* 81:764–70

Koch DL, Shaqfeh E. 1991. Screening in sedimenting suspensions. *J. Fluid Mech.* 224:275–303

Lance M, Bataille J. 1991. Turbulence in the liquid-phase of a uniform bubbly air–water flow. *J. Fluid Mech.* 222:95–118

Magnaudet J, Mougin G. 2007. Wake instability of a fixed spheroidal bubble. *J. Fluid Mech.* 572:311–27

Martínez Mercado J, Chehata Gómez D, Van Gils D, Sun C, Lohse D. 2010. On bubble clustering and energy spectra in pseudo-turbulence. *J. Fluid Mech.* 650:287–306

Martínez Mercado J, Palacios-Morales CA, Zenit R. 2007. Measurement of pseudoturbulence intensity in monodispersed bubbly liquids for $10 < Re < 500$. *Phys. Fluids* 19:103302

Mathai V, Prakash VN, Brons J, Sun C, Lohse D. 2015. Wake-driven dynamics of finite-sized buoyant spheres in turbulence. *Phys. Rev. Lett.* 115:124501

Maxworthy T, Gnann C, Kürten M, Durst F. 1996. Experiments on the rise of air bubbles in clean viscous liquids. *J. Fluid Mech.* 321:421–41

Mazzitelli IM, Lohse D. 2009. Evolution of energy in flow driven by rising bubbles. *Phys. Rev. E* 79:066317

Mendez-Diaz S, Serrano-García JC, Zenit R, Hernández-Cordero JA. 2013. Power spectral distributions of pseudo-turbulent bubbly flows. *Phys. Fluids* 25:043303

Moore DW. 1963. The boundary layer on a spherical gas bubble. *J. Fluid Mech.* 16:161–76

Mudde RF. 2005. Gravity-driven bubbly flows. *Annu. Rev. Fluid Mech.* 37:393–423

Mudde RF, Saito T. 2001. Hydrodynamical similarities between bubble column and bubbly pipe flow. *J. Fluid Mech.* 437:203–28

Parthasarathy RN, Faeth GM. 1990. Turbulence modulation in homogeneous dilute particle-laden flows. *J. Fluid Mech.* 220:485–514

Peters F, Els C. 2012. An experimental study on slow and fast bubbles in tap water. *Chem. Eng. Sci.* 82:194–99

Prakash VN, Martínez Mercado J, van Wijngaarden L, Mancilla E, Tagawa Y, et al. 2016. Energy spectra in turbulent bubbly flows. *J. Fluid Mech.* 791:174–90

Rensen J, Luther S, Lohse D. 2005. The effect of bubbles on developed turbulence. *J. Fluid Mech.* 538:153–87

Riboux G, Legendre D, Risso F. 2013. A model of bubble-induced turbulence based on large-scale wake interactions. *J. Fluid Mech.* 719:362–87

Riboux G, Risso F, Legendre D. 2010. Experimental characterization of the agitation generated by bubbles rising at high Reynolds number. *J. Fluid Mech.* 643:509–39

Risso F. 2011. Theoretical model for k^{-3} spectra in dispersed multiphase flows. *Phys. Fluids* 23:011701

Risso F. 2016. Physical interpretation of probability density functions of bubble-induced agitation. *J. Fluid Mech.* 809:240–63

Risso F, Ellingsen K. 2002. Velocity fluctuations in a homogeneous dilute dispersion of high-Reynolds-number rising bubbles. *J. Fluid Mech.* 453:395–410

Risso F, Roig V, Amoura Z, Riboux G, Billet AM. 2008. Wake attenuation in large Reynolds number dispersed two-phase flows. *Philos. Trans. R. Soc. A* 366:2177–90

Roghair I, Lau YM, Deen NG, Slagter HM, Baltussen MW, et al. 2011a. On the drag force of bubbles in bubble swarms at intermediate and high Reynolds numbers. *Chem. Eng. Sci.* 66:3204–11

Roghair I, Martínez Mercado J, van Sint Annaland M, Kuipers H, Sun C, Lohse D. 2011b. Energy spectra and bubble velocity distributions in pseudo-turbulence: numerical simulations versus experiments. *Int. J. Multiph. Flow* 37:1093–98

Roghair I, van Sint Annaland M, Kuipers HJAM. 2013. Drag force and clustering in bubble swarms. *AIChE J.* 59:1791–800

Roig V, de Tournemine AL. 2007. Measurement of interstitial velocity of homogeneous bubbly flows at low to moderate void fraction. *J. Fluid Mech.* 572:87–24

Roig V, Roudet M, Risso F, Billet AM. 2012. Dynamics of a high-Reynolds-number bubble rising within a thin gap. *J. Fluid Mech.* 707:444–66

Rzehak R, Krepper E. 2013. CFD modeling of bubble-induced turbulence. *Int. J. Multiph. Flow* 55:138–55

Sangani AS, Didwania AK. 2006. Dynamic simulations of flows of bubbly liquids at large Reynolds numbers. *J. Fluid Mech.* 250:307–37

Sato Y, Sadatomi M, Sekoguchi K. 1981. Momentum and heat transfer in two-phase bubble flow. I. Theory. *Int. J. Multiph. Flow* 7:167–77

Shew WL, Poncet S, Pinton JF. 2006. Force measurements on rising bubbles. *J. Fluid Mech.* 569:51–60

Smereka P. 1993. On the motion of bubbles in a periodic box. *J. Fluid Mech.* 254:79–112

Takagi S, Matsumoto Y. 2011. Surfactant effects on bubble motion and bubbly flows. *Annu. Rev. Fluid Mech.* 43:615–36

Takagi S, Ogasawara T, Matsumoto Y. 2008. The effects of surfactant on the multiscale structure of bubbly flows. *Philos. Trans. R. Soc. A* 366:2117–29

Tennekes H, Lumley JL. 1972. *A First Course in Turbulence*. Cambridge, MA: MIT Press

Vélez-Cordero JR, Lantenet J, Hernández-Cordero J, Zenit R. 2014. Compact bubble clusters in Newtonian and non-Newtonian liquids. *Phys. Fluids* 26:053101

Yurkovetsky Y, Brady JF. 1996. Statistical mechanics of bubbly liquids. *Phys. Fluids* 8:881–95

Zenit R, Koch DL, Sangani AS. 2001. Measurements of the average properties of a suspension of bubbles rising in a vertical channel. *J. Fluid Mech.* 429:307–42

Zenit R, Magnaudet J. 2008. Path instability of rising spheroidal air bubbles: a shape-controlled process. *Phys. Fluids* 20:061702

Ziegenhein T, Rzehak R, Ma T, Lucas D. 2017. Towards a unified approach for modelling uniform and non-uniform bubbly flows. *Can. J. Chem. Eng.* 95:170–79

Contents

Indexes

Errata

An online log of corrections to *Annual Review of Fluid Mechanics* articles may be found at http://www.annualreviews.org/errata/fluid